THE JOURNAL OF PHYSICAL CHEMIST

Article

Mechanism of Inhibition of Cholesteryl Ester Transfer Protein by Small Molecule Inhibitors

Venkat Reddy Chirasani, Revathi Sankar, and Sanjib Senapati

J. Phys. Chem. B, **Just Accepted Manuscript** • DOI: 10.1021/acs.jpcb.6b01928 • Publication Date (Web): 25 Apr 2016

ACS Publications

The Journal of Physical Chemistry B is published by the American Chemical Society. 1155 Sixteenth Street N.W., Washington, DC 20036

Mechanism of Inhibition of Cholesteryl Ester Transfer Protein by Small Molecule Inhibitors

Venkat R. Chirasani, Revathi Sankar, and Sanjib Senapati*

Bhupat and Jyoti Mehta School of Biosciences and Department of Biotechnology, Indian Institute of Technology Madras, Chennai 600036, India

Phone: +91-44-2257-4122. Fax: +91-44-2257-4102. E-mail: sanjibs@iitm.ac.in.

ABSTRACT

Cholesteryl ester transfer protein (CETP) facilitates the bidirectional exchange of cholesteryl esters and triglycerides between High Density Lipoproteins (HDL) and Low or Very Low Density Lipoproteins (LDL/VLDL). Recent studies have shown that the impairment of lipid exchange processes of CETP can be an effective strategy for the treatment of cardiovascular diseases (CVD). Understanding the molecular mechanism of CETP inhibition has, therefore, attracted tremendous attention in recent past. In this study, we explored the detailed mechanism of CETP inhibition by a series of recently reported small molecule inhibitors that are currently under pre-clinical testing. Our results from molecular dynamics (MD) simulations and protein-ligand docking studies suggest that the hydrophobic interactions between the CETP core tunnel residues and inhibitor moieties play a pivotal role, and physical occlusion of the CETP tunnel by these small molecules is the primary mechanism of CETP inhibition. Interestingly, bound inhibitors were found to increase the plasticity of CETP, which was explained by principal component analysis that showed a larger space of sampling of CETP C-domain due to inhibitor binding. The atomic-level details presented here could help accelerating the structure-based drug discovery processes targeting CETP for CVD therapeutics.

INTRODUCTION

Cholesteryl Ester Transfer Protein (CETP) plays an indispensable role in lipid metabolism by facilitating the transfer of neutral lipids between various lipoprotein particles like High Density Lipoproteins (HDL), Low Density Lipoproteins (LDL) and Very Low Density Lipoproteins (VLDL). The net lipid transfer mediated by CETP is the bidirectional exchange of cholesteryl esters (CEs) from HDL to LDL, with a reciprocal transport of triglycerides (TGs) in the opposite direction.[1] Deficiency of CETP and its inhibition in humans and rabbits have shown a reduced susceptibility to the development of atherosclerosis.[2–4] Furthermore, human subjects with heterozygous CETP deficiency also have demonstrated a reduced susceptibility to the development of coronary heart diseases.[5,6] This reduced risk is shown due to the enrichment of HDL-CEs with a simultaneous depletion of the LDL-CEs upon CETP inhibition, thus leading to a typical atheroprotective profile. Since then CETP has been actively pursued as a therapeutic target for the prevention and treatment of cardiovascular diseases (CVDs).

Usage of small molecule drugs to inhibit CETP's lipid transfer activity and hence to raise human plasma HDL-CE levels has been pursued as an active approach to prevent cardiovascular diseases over the past decade.[7–10] Despite the role of statins in the significant suppression of LDL-CE levels, cardiovascular disease is still the primary cause of increase in mortality rate across the world.[11] Out of many small chemical compounds tested for CETP inhibition activity, four had entered into clinical testing: torcetrapib,[12] dalcetrapib (R1658),[3] anacetrapib (MK-859),[13] and evacetrapib (LY2484595).[14] However, the clinical trials of torcetrapib were terminated due to its adverse side effects and increased mortality rate.[15,16] In the same line, dalcetrapib and evacetrapib were also discontinued from clinical testing phase due to their futility in raising HDL levels.[17,18] Recently, a new CETP inhibitor, BMS-795311 advanced into pre-clinical safety studies with minimal side effects.[19] Thus, anacetrapib and BMS-795311 with an acceptable side-effect profile are still under pre-clinical/clinical phase studies.

Given the importance of CETP inhibition in the prevention and treatment of CVDs, understanding the nature of interactions of small molecules with CETP at the atomic level may illuminate our understanding of how these compounds inhibit CETP. Valuable insights were obtained from the X-ray crystal structure of substrate-bound CETP in 2007 (PDB ID: 2OBD),[20] which showed the protein to be a *'boomerang'* shaped molecule possessing a high degree of structural homology to the family of lipid binding and/or transporting proteins, including FABP[21], BPI[22], PLTP[23] etc. CETP is a pseudo dimer with similar N- and C-terminal beta barrel domains, interfaced by a central beta domain (Fig. 1a). Each of the N- and C-terminal beta barrel domain contains a twisted beta sheet and two helices. N-terminal domain contains five beta strands: S2 -S6, two helices: helix-A and helix-B, and three functionally important loop regions: Ω4, Ω5, and Ω6. Similarly, the C-terminal domain comprises of five twisted beta strands, three helices, and three loop regions: Ω1, Ω2, and Ω3. The central beta domain contains six anti-parallel beta strands: S1, S7, S8, S1′, S7′, and S8′. Unlike other lipid transporting proteins, CETP also possesses a flexible linker at the central beta domain and an amphipathic helix, helix-X at the C-terminus. Helix-X is thought to play a significant role in the lipid transport action of CETP[24] and inhibitor entry.[25] Moreover, the crystal structure illustrated the presence of four bound lipid molecules - two cholesteryl esters (CEs) and two phospholipids (PLs). These lipids are accommodated in a 60 Å long hydrophobic tunnel that traverses through the core of CETP.

The continuous increase in the number of patents and research articles on developing new classes of CETP inhibitors is indicative of the growing interest in CETP inhibition.[26,27] The fairly recent crystal structure of torcetrapib bound CETP (PDB ID: 4EWS)[28] shows that the inhibitor binds to the N-terminal pocket of the CETP tunnel and displaces N-terminal phospholipid (PL-1) to gain access into the CETP hydrophobic tunnel. Even though this structure has provided wealth of information about the interactions of torcetrapib with CETP, our understanding of the mechanism of CETP inhibition by small molecule inhibitors is still far from complete. Here, we present a comparative study of the interactions of torcetrapib and two promising inhibitors, anacetrapib and BMS-795311 with CETP by employing molecular dynamics (MD) simulations and protein–ligand docking studies. Results are compared with substrate bound CETP simulation data to gain deeper insights. Our results suggest that the physical occlusion of the CETP core tunnel by the bound small molecules is the primary mechanism of CETP inhibition. Results also suggest that inhibitor binding enhances the flexibility, particularly of the C-terminal domain of CETP significantly. Moreover, our study identified common interactions among the three CETP-inhibitor complexes, which might help designing future mutagenesis studies.

METHODS

Molecular dynamics simulations

We started the MD simulations of torcetrapib- (*ethyl (2R,4S)-4-({[3,5-bis(trifluoromethyl)phenyl]methyl}(methoxycarbonyl)amino)-2-ethyl-6-(trifluoromethyl) 1,2,3,4-tetrahydroquinoline-1-carboxylate;* Fig. 1b) bound CETP from the available crystal structure with PDB ID: 4EWS.[28] After thorough equilibration, the system was simulated for 200 ns at 310K and 1 atm. As a control, substrate-bound CETP (PDB ID: 2OBD[20]) is also simulated for 200ns. Since the structures of anacetrapib- *((4S,5R)-5-[3,5-bis(trifluoromethyl)phenyl]-3-({2-[4-fluoro-2-methoxy-5-(propan-2-yl)phenyl]-5-(trifluoromethyl)phenyl}methyl)-4-methyl-1,3-oxazolidin-2-one*; Fig. 1c) bound CETP and BMS-795311-(*N-[(1R)-1-(3-cyclopropoxy-4-fluorophenyl)-1-[3-fluoro-5-(1,1,2,2-tetrafluoroethoxy)phenyl]-2-phenylethyl]-4-fluoro-3-(trifluoromethyl)benzamide*; Fig. 1d) bound CETP were not known, we initially performed the protein-ligand docking using Autodock-4.2[29] by considering torcetrapib-bound CETP as the reference structure and subsequently performed MD simulations on these complexes for 200ns each. Before this, the chemical structures of anacetrapib and BMS-795311 were optimised with Gaussian 09 program with B3LYP functional and 6–311+G* basis set.[30] The optimized conformations of anacetrapib and BMS-795311 were subsequently docked on CETP to generate the initial configurations for simulation studies. It is to be noted that, while performing the docking studies, the N-terminal phospholipid was excluded from CETP structure, following the solved structure of torcetrapib-bound CETP,[28] where the N-terminal phospholipid was displaced by the inhibitor. Gasteiger charges and rotatable bonds were assigned using Autodock tools to the inhibitors. The grid box was centered on torcetrapib binding site in the hydrophobic tunnel with dimensions 66 Å x 66 Å x 66 Å, such that it effectively covers the inhibitor binding pocket. Lamarckian genetic algorithm (LGA) with 25,00,000 energy assessments was accomplished to identify the best binding pose of ligand into the protein. The final docked conformations were clustered using a tolerance of 1 Å root-mean-square deviation (RMSD). The best binding poses for anacetrapib and BMS-795311 were chosen based on their similarity in relative orientation of torcetrapib in the crystal structure of torcetrapib-CETP complex, along with the binding energy score.

Before performing the MD simulations, the N-terminal missing residues, ALA1, SER2, LYS3, and GLY4 in substrate bound and inhibitor bound crystal structures, were incorporated with the help of MODELLER9v13.[31] Subsequently, the mutations induced in

CETP during crystallization, viz. C1A, N88D, C131A, N240D, and N341D were mutated back to generate the wild type CETP structures. Noting that the tail of the N-terminal cholesteryl ester was missing in the crystal structure of torcetrapib-CETP complex, we added those atoms and performed extensive minimisation and thermalisation to allow the system to remediate the bad geometry. GROMOS53A6 forcefield[32] for CETP and Berger lipid parameters for CEs and PLs were obtained from literature.[33–35] GROMOS53A6 compatible forcefield parameters for torcetrapib, anacetrapib and BMS-795311 were obtained from ATB server.[36] The atom-centred RESP charges for inhibitors *viz* torcetrapib, anacetrapib, and BMS-795311 were obtained via fits to the electrostatic potentials acquired from the calculated wave functions.[30] The protonation states of CETP histidines - HSD or HSE - were deduced by the local hydrogen bonding network using WHATIF program.[37] After the gas phase relaxation, the CETP-ligand complexes were solvated in a cubic box of explicit water. Water molecules were distributed in such a way that they extend up to 12 Å from the protein-ligand surface in all X-, Y-, and Z-directions. Water molecules were described by SPC water model and ionic strength of 0.15 M NaCl was maintained by adding appropriate number of Na^+ and Cl^- ions. Long-range electrostatics were treated using particle-mesh Ewald sum with a cut-off of 10 Å.[38] To mimic physiological conditions, the temperature was kept at 310K by using V-rescale thermostat with a coupling constant of 0.1 ps. Parrinello-Rahman barostat with isotropic pressure coupling was used using a coupling constant of 0.1ps to maintain the pressure at 1 atm. All systems were then equilibrated in NPT ensemble with time step of 2 fs for 20 ns. During this equilibration phase, the energy components, mass density, and root-mean-square-deviations converged. The resulting structures were simulated for 200 ns each to generate the MD data. All simulations were performed on 128 processors of an Infiniband Xeon E5-2670 linux cluster using GROMACS-5.0.4 simulation package.[39]

Principal Component Analysis

Principal component analysis (PCA) is employed to explore the dominant motions of CETP-ligand complexes.[40] PCA transforms the correlated protein motions into a reduced space of independent motions by calculating and, subsequently, diagonalizing the covariance matrix, C_{ij} of the positional deviations of protein residues. The details of PCA methodology can be found in Ref. 41. The principal component analysis was performed using g_covar module in GROMACS. The porcupine plots were generated using a Tcl script in VMD.[42] These plots depict a graphical representation of the dominant protein motions. The porcupine plots were rendered using VMD by drawing a cone for each CETP residue corresponding to the direction of its movement.

CAVER 3.0 program was used to identify and characterize the tunnels in substrate and inhibitor bound CETP trajectories.[43] CAVER calculates Voronoi diagram of the atomic centers and identifies tunnels as shortest paths between all pairs of points using Dijkstra's algorithm. Various conformations of CETP excluding lipid components were considered for tunnel analysis and the probe radius was set to 3Å to construct molecular surface of pocket or tunnel. VMD[42] was employed to generate all structural figures. LigPlot^{+} tool[44] was used to capture the 2D protein-inhibitor interactions profile.

RESULTS AND DISCUSSION

Protein-ligand docking results reproduced the crystal conformation of inhibitor binding

We performed all-atom, unrestrained MD simulations of a series of inhibitor-bound CETP to understand the detailed mechanism of CETP inhibition. As a control, substrate-bound CETP is also simulated to compare the changes in structure and dynamics of the protein. The simulations of torcetrapib- and substrate-bound CETP were started from the available crystal structures. However, in absence of any structural information of CETP bound to anacetrapib and BMS-795311 inhibitors, we modelled their initial structures by performing protein-ligand docking studies. These structures were subsequently refined by MD simulations, following the same protocol used for torcetrapib- and substrate-bound CETP. Results are then compared over the 200ns production phase.

For the protein-ligand docking studies, we first devised the correct protocol by docking torcetrapib to the crystal conformation of CETP. To obtain this, we first removed torcetrapib from the torcetrapib-CETP crystal structure and then allowed torcetrapib to explore all possible conformations by introducing inherent flexibility in its structure. The generated set of torcetrapib conformers were then allowed to explore the binding pocket of CETP in crystal conformation. Interestingly, the docking results reproduced the crystal structure of torcetrapib-CETP complex very well with the most favorable free energy complex (-10.70 kcal/mol) showing the exact pose of torcetrapib in the crystal structure (Fig. S1). The Root Mean Square deviation (RMSD) of this lowest free energy conformation of torcetrapib from crystal structure was only 1.44 Å. This close resemblance of torcetrapib binding to CETP validates our docking protocol. Subsequently, we performed docking of anacetrapib and BMS-795311 with the exact same set of docking parameters and grid-box dimension. When the flexible anacetrapib and BMS-795311 were docked into the CETP inhibitor binding pocket, both molecules acquired the binding pose very similar to that of the torcetrapib. Respective binding free energy of -11.73 kcal mol^{-1} and -11.05 kcal mol^{-1} also matched very well with that of torcetrapib (-10.70 kcal mol^{-1}), in consistent with their similar IC_{50} values (Table 1). For a better comparison with the experimental data, we have estimated experimental binding free energy from IC_{50} values by assuming that binding of these inhibitors to CETP follows the noncompetitive kinetics, and under such circumstances IC_{50} equals to the inhibition constant, K_i and the relation $\Delta G = -RT\, ln(IC_{50})$ stands valid.[45] Interestingly, the recent biochemical studies on CETP have suggested non-competitive inhibition of the torcetrapib series of inhibitors to CETP.[46]

Inhibitor binding enhances the protein dynamics

Primarily we have performed four independent MD simulations of inhibitor and substrate bound CETP for 200ns each. Table S1 lists all the systems simulated in this work. Before performing analyses on the simulation trajectories, it is important to make sure that the systems were well equilibrated. Hence, we monitored the root mean square deviations (RMSD) of the protein in each complex relative to its crystal conformation and the results are shown in Fig. S2a. As the figure shows, all the complexes attained stability quickly within the initial 50 ns. Hence, the subsequent analyses were performed on the final 150 ns data of all the systems. To check the stability of the binding modes of inhibitors in CETP tunnel, we also have calculated RMSD of the ligands along the MD trajectories (Fig. S2b). The small RMSD values averaging around 0.15 nm are suggestive of their stable binding to CETP. The relatively larger RMSD of the protein is presumably due to significant relaxations of the bound substrates from crystal structure (crystal packing effects). Interestingly, a recent MD simulation study using OPLS-AA force field has also reported similar large RMSD values for both CETP and its substrates.[47]

To understand the effect of inhibitor binding on the local fluctuation of CETP residues, we compared the root-mean-square fluctuations (RMSF) of the protein residues in inhibitor and substrate bound states. RMSF measures the relative internal motions of the protein residues and high RMSF values for a region imply that this particular region is more flexible in comparison to the regions possessing low RMSF values. Fig. 2 compares the RMSF values of CETP residues in substrate and inhibitor bound states. The average RMSF profile, as presented in this figure, is obtained by averaging over fifteen individual RMSF profiles generated from each 10 ns of the 150 ns production data to reduce the statistical error. It is evident from this figure that the presence of inhibitors increased the flexibility of CETP compared to that in substrate-bound CETP (*i.e.* CETP without inhibitor). This is quite interesting, since inhibitor binding usually suppresses the motions in protein. However, the present study showed an opposite trend, where inhibitor binding has substantially elevated the dynamics of CETP, particularly in its C-terminal and linker domains. The inhibitor binding also resulted in enhanced mobility of the amphipathic helix, helix-X. Previous studies have implicated the role of helix-X in substrate transfer and inhibitor uptake.[24,25] The C-terminal distal loops, Ω1-Ω3 that showed large fluctuations due to inhibitor binding are also known to be functionally relevant and involve in lipoprotein binding.[48] Thus, it is evident that the inhibitor binding modulates the flexibility of the functionally important regions of CETP, which may have a direct or indirect impact on the function of the protein. It is worth noting that the inhibitor binding decreased the flexibility of the residues located around the inhibitor in CETP N-terminal domain, including that of the N-terminal highly fluctuating loops, Ω4-Ω6. Nevertheless, the overall flexibility of CETP was increased due to inhibitor binding as will be shown more quantitatively in later section by principal component analysis.

Inhibitors interact mostly with the CETP hydrophobic tunnel residues

The binding similarity among the inhibitors with CETP is already evident from molecular docking studies. However, to understand the common interactions at residue-level, we have extracted the time-averaged structures of inhibitor bound CETP from respective simulation trajectory. Fig. 3 presents the three-dimensional distributions of protein residues around the inhibitors in CETP binding pocket. Residues that fall within 3.5 Å from inhibitor surface are considered, which therefore include all protein residues interacting with the inhibitor moieties by H-bond and van der Waals interactions. Interestingly, majority of the interacting protein residues were found to be hydrophobic in all inhibitor-CETP complexes. More importantly, many of these interacting residues were common in all three complexes.

Similar to the torcetrapib-CETP crystal structure, all three inhibitors were located in the hydrophobic N-terminal pocket of CETP, comprised partly by N-terminal beta strands: S5, S6, helix-B, and central domain beta strand S8.[20] Further, the deep penetration of the central phenyl-fluoromethyl along with the neighboring –N-C=O moiety of the inhibitors (this central moiety of inhibitors is depicted in Fig. 1) have explored a sub-pocket constituted by the aromatic rings of H232, F263, hydrophobic side chains of I11, C13, I15, and L261 that belong to the CETP central beta domain region. Further, all three inhibitors were involved in hydrophobic interactions with helix-B residues: Q199, A202, I205; N-terminal domain residue I215; and S6 strand residue V136. Despite the highly hydrophobic nature of the N-terminal pocket, three polar residues were observed to be present around the inhibitor binding pocket, *viz* Q199, S230, and H232. Overall, a significant number of 85.71% similar residues were found to be located around all three inhibitors studied. The commonality in interacting residues between the simulated and crystal structures of torcetrapib bound CETP was 78.57%.

Both torcetrapib and anacetrapib possessed additional hydrophobic interactions with the N-terminal pocket capping residue: F441. Likewise, anacetrapib and BMS-795311 displayed additional hydrophobic interactions with helix-B residues: A195 and V198. Additionally, torcetrapib and BMS-795311 have common hydrophobic interactions with the central beta domain residue: S230. While anacetrapib exhibited additional interactions with S5 strand residue: L129; N-terminal pocket opening residue: R201; and central beta domain residue: L228, BMS-795311 involved in hydrophobic interactions with the S6 strand residues: G134, R135, T138; N-terminal domain residues: L217, P221; C-terminal capping residue of helix-B: L206; and central beta domain residue: F265. It is noteworthy that the trifluoromethyl group in anacetrapib was involved in hydrogen bonding with Q199. Such a hydrogen bond formation in highly hydrophobic environment is thought to compensate the dehydration penalty incurred due to the burial of hydrophilic group and contributes to favorable binding of the inhibitor. It is also interesting to note that, all inhibitors have strong hydrophobic association with the oleoyl tail of CE-1, as was also noted in the torcetrapib-CETP crystal structure. However, this is masked in Fig. 3 for visual clarity. Moreover, the residues C13, H232, and F263 that were reported to be crucial in torcetrapib binding from alanine mutational study[28], were found to have identical interactions with all three inhibitors studied as discussed above, thus further validating their similar mode of interactions.

Inhibitors physically block the CETP core tunnel

To understand the mechanism of CETP inhibition by this class of inhibitors, next we investigated the evolution of CETP core tunnel in substrate-bound *versus* inhibitor-bound states. As noted in the crystal structure of substrate bound CETP, the protein possesses a core tunnel of length 60 Å and volume 2560 Å^3, where the cholesteryl esters are loaded.[20] However, the tunnel information was not reported in the torcetrapib-bound CETP crystal structure. We have computed the tunnel length of CETP in different states by CAVER program, which identifies tunnels by mapping Voronoi diagram of the atomic centers and then calculating the shortest paths between all pairs of points. Fig. 4a presents the length and radius of CETP hydrophobic tunnel in substrate-bound and inhibitor-bound states. The tunnel of the substrate-bound CETP crystal structure is well reproduced with a length of 65Å (black dotted line in Fig. 4a). When this length is compared with that of the same substrate-bound CETP from MD simulation data, a striking difference was observed. A continuous tunnel of length 110 Å with volume 3536 Å^3 and tunnel radius ~1.4 Å larger than the crystal structure was noted. We speculate that the shorter tunnel length in CETP crystal structure is due to the crystal packing effects and when simulated in water, the protein structure relaxes from crystal packing to evolve a much larger tunnel. This finding also goes parallel to the study of Zhang et al, where the authors found CETP to exist in an "open-state" having a continuous tunnel similar to ours (Fig. S13 of Ref. 48).

As Fig. 4a also shows, the tunnel length for all the inhibitor-bound CETP time-averaged structures is only about 70 Å with volume approximately 2700 Å^3. This significant reduction in tunnel length and volume suggests that the inhibitors occupy the tunnel and block the passage necessary for substrate transfer. To get a clearer understanding, we have rendered the 3D representation of the CETP tunnel in absence and presence of the inhibitors and presented the results in Figures 4b and 4c. It is evident from these figures that the inhibitors bind almost at the center of the CETP hydrophobic tunnel and make the tunnel very constricted. As a result, the transfer of cholesteryl esters and triglycerides, the CETP substrates becomes very inefficient and the protein looses the activity. Thus, based on the position and nature of protein contacts exploited by the inhibitors, physical occlusion of the channel is found to be the primary mechanism of CETP inhibition.

To validate our findings of protein-inhibitor interactions and the evolution of CETP core tunnel in presence of the inhibitors, we have performed a second set of substrate-bound CETP and inhibitor-bound CETP simulations. Each of the substrate-bound and three inhibitor-bound CETP complexes was also simulated for 200ns. The simulations were started with the same initial structures as that of the primary simulations, but with different initial velocity assigned from Maxwell-Boltzmann distributions. The details of these systems are included in Table S1. Fig. 5 shows the time-averaged distributions of the interacting CETP residues around the inhibitors, in this new set of simulations. Here, we displayed the protein-ligand 2D structural representation by performing LigPlot analysis. Interestingly, both set of simulations captured the same set of CETP residues interacting with the inhibitors. Particularly, the deep penetration of phenyl-fluoromethyl group with –N-C=O moiety of the inhibitors into CETP sub-pocket formed by central beta domain residues C13, I15, S230, and H232 was again evident. The strong interaction of helix-B residues Q199, A202, I205and stacking interaction of F263 with one of the middle phenyl rings in the inhibitors, as depicted in Fig. 3 from primary set of simulations, were also well reproduced. Overall, a significant overlap of the interaction pattern was observed from two independent sets of simulations.

We have also examined the evolution of CETP tunnel from the second set of simulations. Fig. S3 presents the length and radius of CETP hydrophobic tunnel in the time-averaged structures of inhibitor-CETP complexes from respective simulations. The plot depicts tunnels of length between 66Å - 72 Å with average volume ~2811 Å^3 in all inhibitor-bound CETP systems, similar to the tunnel dimensions obtained from first set of simulations. To have a better visualization, we have sliced the protein at the center of mass and looked through the tunnel from N-terminal end. The 3D representations are included in Figures S3b and S3c. It is again apparent from these figures that the binding of inhibitors physically blocks the tunnel and thus can obstruct the movements of neutral lipids effectively. Hence, the physical occlusion of CETP tunnel appears to be the mechanism of CETP inhibition by this class of inhibitors. It is worth mentioning here that CETP explored a range of conformations during the MD simulations, and correspondingly the tunnel length varied from 65 Å - 112 Å in substrate-bound CETP and 42 Å - 77 Å in inhibitor-bound CETP. The shorter tunnels appear particularly when CETP bends and its core tunnel become discontinuous with multiple short tunnels. For comparison in Fig. 3 and S3, we picked up the cluster of longer tunnels from each system and averaged over them. While doing so, we made sure that each cluster of long tunnels was comprised of minimum of 25% of the conformations that CETP had explored during simulations.

Principal component analysis could explain the basis of increased CETP dynamics

Finally, to understand the basis for increased CETP dynamics in presence of the inhibitors, we resorted to Principal Component Analysis (PCA) to identify the essential motions in the protein. The advantage of PCA is that it allows the identification of dominant modes of protein motions by extracting smaller number of independent variables (principal components) from a larger set of correlated variables. Fig. S4 depicts the relative contributions of various principal motions (eigenvectors) to the overall dynamics of the protein. The figure clearly indicates that a small number of eigenvectors (collective motions of the atoms) are enough to describe the bulk of the protein dynamics. The first ten principal components describe ~77%, ~76%, ~78.3%, and ~77.6% of the total mean-square fluctuations in the substrate, torcetrapib, anacetrapib, and BMS-795311 bound systems (Fig. S4 inset). The inset also shows that the first eigenvector contributes significantly; representing ~49.5%, ~44.9%, ~52.7%, and ~53.4% of the total fluctuations in the substrate, torcetrapib, anacetrapib, and BMS-795311 bound states. To compare conformational space sampled by the substrate and inhibitor-bound CETP systems, two-dimensional projections of MD ensembles onto the plane defined by the first two eigenvectors are plotted (Fig. S5). Although the regions explored by the four systems overlap, the dynamics of the inhibitor-bound CETP spans larger space in comparison to that of the substrate-bound CETP (68.55 nm^2 in substrate-CETP *vs* 85.63 nm^2 in BMS-795311 bound CETP). Similar trend was noted from the PCA on second set of simulations data also. This observation is consistent with the results in Fig. 2, where the protein displayed increased dynamics in presence of the inhibitors. The complementarity between the RMSF and PCA results indicates, the CETP residues that exhibited large RMS fluctuations contribute significantly to the essential motions of the protein.

The principal motions of protein residues can be better visualized by representing the eigenvectors as porcupine plots. In Fig. 6, we presented the motion of CETP residues along the direction of principal component 1 (PC1). In this plot, the length of the cones (representing the eigenvectors) denotes the magnitude and the projection identifies the direction of motions of the protein residues. Two interesting features emerged from the principal motions of CETP residues. The N-domain, particularly the ligand binding site underwent reduced flexibility in presence of the inhibitors compared to the substrate-bound CETP. This is expected as the favorable binding of ligands imparts local stability to the protein domain. Interestingly however, all other regions in the protein, e.g. C-terminal loop regions Ω1- Ω3, C-terminal beta barrel domain, central linker region exhibited significantly larger average velocity covariance vectors in the inhibitor-bound complexes than the substrate-bound CETP. The overall effect of inhibitor binding, therefore, sums up to increased dynamics in the protein. The largest dynamics in BMS-795311 bound CETP system could be due to the bulkiness of BMS-795311 compared to other inhibitors. We speculate that one of the main reasons for increased plasticity in CETP could be the asymmetry in the structure imparted by inhibitor binding. This will be our focus for future study. The study also paves way to explore the signaling pathways by which the inhibitor binding in N-domain modulates the dynamics of distal C-domain regions, such as loops Ω1-Ω3 etc.

CONCLUSIONS

CETP mediates the net transfer of CEs from HDL to LDL with a reciprocal transport of TGs from LDL to HDL. Deficiency of CETP and its inhibition in humans and rabbits have shown a reduced susceptibility to the development of atherosclerosis. Hence, CETP is actively pursued as a therapeutic target for the treatment of cardiovascular diseases. Even though the recent torcetrapib-bound CETP crystal structure has provided wealth of information about the interactions of torcetrapib with CETP, our understanding of the mechanism of CETP inhibition by small molecule inhibitors is still far from complete. Here, we present a comparative study of the interactions of torcetrapib and two promising CETP inhibitors, anacetrapib and BMS-795311 with CETP by employing molecular dynamics (MD) simulations, protein – ligand docking, and principal component analysis. Results are compared with substrate bound CETP simulation data to gain deeper insights. Our results suggest that the physical occlusion of the CETP core tunnel by the bound small molecule inhibitors is the primary mechanism of CETP inhibition. Results also suggest that multiple hydrophobic, H-bond, and ring stacking interactions between CETP tunnel lining residues and the inhibitors are responsible for nanomolar binding of the inhibitors to CETP. The study also identified multiple common interactions among the three CETP-inhibitor complexes studied here, which can be tested experimentally by mutagenesis studies. Interestingly, the inhibitor binding was shown to enhance the CETP dynamics significantly, particularly of its C-terminal domain. We speculate that one of the primary reasons for increased plasticity in CETP could be due to imparted asymmetry in the structure by inhibitor binding. This will be our focus for future study.

SUPPORTING INFORMATION

Figure S1 shows the comparison of the binding pose of torcetrapib in CETP crystal structure and in the lowest energy docked complex of torcetrapib-CETP. Figures S2 shows the time evolution of root mean square deviations (RMSDs) of CETP and its bound ligands. Figure S3 shows the evolution of CETP core tunnel in replica simulations. Figure S4 shows the eigenvalue profile of essential dynamics and the cumulative contribution of eigenvectors in substrate bound and inhibitor bound CETP simulations. Figure S5 depicts two-dimensional projections of the simulated structures from principal component analysis. Table S1 presents the list of systems studied.

ACKNOWLEDGEMENTS

We would like to thank the High Performance Computing Environment (HPCE), IIT Madras for providing computational resources.

REFERENCES

(1) Barter, P. J. Cholesteryl Ester Transfer Protein: A Novel Target for Raising HDL and Inhibiting Atherosclerosis. *Arterioscler. Thromb. Vasc. Biol.* **2003**, *23*, 160–167.

(2) Zhong, S.; Sharp, D. S.; Grove, J. S.; Bruce, C.; Yano, K.; Curb, J. D.; Tall, A. R. Increased Coronary Heart Disease in Japanese-American Men with Mutation in the Cholesteryl Ester Transfer Protein Gene despite Increased HDL Levels. *J. Clin. Invest.* **1996**, *97*, 2917–2923.

(3) Okamoto, H.; Yonemori, F.; Wakitani, K.; Minowa, T.; Maeda, K.; Shinkai, H. A Cholesteryl Ester Transfer Protein Inhibitor Attenuates Atherosclerosis in Rabbits. *Nature* **2000**, *406*, 203–207.

(4) Morehouse, L. a; Sugarman, E. D.; Bourassa, P.-A.; Sand, T. M.; Zimetti, F.; Gao, F.; Rothblat, G. H.; Milici, A. J. Inhibition of CETP Activity by Torcetrapib Reduces Susceptibility to Diet-Induced Atherosclerosis in New Zealand White Rabbits. *J. Lipid Res.* **2007**, *48*, 1263–1272.

(5) Gordon, T.; Castelli, W. P.; Hjortland, M. C.; Kannel, W. B.; Dawber, T. R. High Density Lipoprotein as a Protective Factor against Coronary Heart Disease. *Am. J. Med.* **1977**, *62*, 707–714.

(6) Inazu, A.; Brown, M. L.; Hesler, C. B.; Agellon, L. B.; Koizumi, J.; Takata, K.; Maruhama, Y.; Mabuchi, H.; Tall, A. R. Increased High-Density Lipoprotein Levels Caused by a Common Cholesteryl-Ester Transfer Protein Gene Mutation. *N. Engl. J. Med.* **1990**, *323*, 1234–1238.

(7) Linsel-Nitschke, P.; Tall, A. R. HDL as a Target in the Treatment of Atherosclerotic Cardiovascular Disease. *Nat. Rev. Drug Discov.* **2005**, *4*, 193–205.

(8) Dullaart, R. P. F.; Dallinga-Thie, G. M.; Wolffenbuttel, B. H. R.; van Tol, A. CETP Inhibition in Cardiovascular Risk Management: A Critical Appraisal. *Eur. J. Clin. Invest.* **2007**, *37*, 90–98.

(9) Joy, T.; Hegele, R. A. Is Raising HDL a Futile Strategy for Atheroprotection? *Nat.*

Rev. Drug Discov. **2008**, *7*, 143–155.

(10) Cannon, C. P. HIgh-Density Lipoprotein Cholesterol as the Holy Grail. *JAMA* **2011**, *306*, 2153–2155.

(11) The Atlas of Heart Disease and Stroke*,* **2008**, *World Health Organization*, Geneva, Switzerland.

(12) Ruggeri, R. B. Cholesteryl Ester Transfer Protein: Pharmacological Inhibition for the Modulation of Plasma Cholesterol Levels and Promising Target for the Prevention of Atherosclerosis. *Curr. Top Med. Chem*. **2005**, *5*, 257–264.

(13) Krishna, R.; Anderson, M. S.; Bergman, A. J.; Jin, B.; Fallon, M.; Cote, J.; Rosko, K.; Chavez-Eng, C.; Lutz, R.; Bloomfield, D. M.; et al. Effect of the Cholesteryl Ester Transfer Protein Inhibitor, Anacetrapib, on Lipoproteins in Patients with Dyslipidaemia and on 24-H Ambulatory Blood Pressure in Healthy Individuals: Two Double-Blind, Randomised Placebo-Controlled Phase I Studies. *Lancet* **2007**, *370*, 1907–1914.

(14) Cao, G.; Beyer, T. P.; Zhang, Y.; Schmidt, R. J.; Chen, Y. Q.; Cockerham, S. L.; Zimmerman, K. M.; Karathanasis, S. K.; Cannady, E. A.; Fields, T.; et al. Evacetrapib Is a Novel, Potent, and Selective Inhibitor of Cholesteryl Ester Transfer Protein That Elevates HDL Cholesterol without Inducing Aldosterone or Increasing Blood Pressure. *J. Lipid Res.* **2011**, *52*, 2169–2176.

(15) Barter, P. J.; Caulfield, M.; Eriksson, M.; Grundy, S. M.; Kastelein, J. J. P.; Komajda, M.; Lopez-Sendon, J.; Mosca, L.; Tardif, J.-C.; Waters, D. D.; et al. Effects of Torcetrapib in Patients at High Risk for Coronary Events. *N. Engl. J. Med.* **2007**, *357*, 2109–2122.

(16) Bots, M. L.; Visseren, F. L.; Evans, G. W.; Riley, W. A.; Revkin, J. H.; Tegeler, C. H.; Shear, C. L.; Duggan, W. T.; Vicari, R. M.; Grobbee, D. E.; et al. Torcetrapib and Carotid Intima-Media Thickness in Mixed Dyslipidaemia (RADIANCE 2 Study): A Randomised, Double-Blind Trial. *Lancet* **2016**, *370*, 153–160.

(17) Schwartz, G. G.; Olsson, A. G.; Abt, M.; Ballantyne, C. M.; Barter, P. J.; Brumm, J.;

Chaitman, B. R.; Holme, I. M.; Kallend, D.; Leiter, L. A.; et al. Effects of Dalcetrapib in Patients with a Recent Acute Coronary Syndrome. *N. Engl. J. Med.* **2012**, *367*, 2089–2099.

(18) Mullard, A. CETP Set-Back, Again. *Nat. Rev. Drug Discov.* **2015**, *14*, 739–739.

(19) Qiao, J. X.; Wang, T. C.; Adam, L. P.; Chen, A. Y. A.; Taylor, D. S.; Yang, R. Z.; Zhuang, S.; Sleph, P. G.; Li, J. P.; Li, D.; et al. Triphenylethanamine Derivatives as Cholesteryl Ester Transfer Protein Inhibitors: Discovery of N-[(1R)-1-(3-Cyclopropoxy-4-Fluorophenyl)-1-[3-Fluoro-5-(1,1,2,2-Tetrafluoroethoxy)phenyl]-2-Phenylethyl]-4-Fluoro-3-(Trifluoromethyl)benzamide (BMS-795311). *J. Med. Chem.* **2015**, *58*, 9010–9026.

(20) Qiu, X.; Mistry, A.; Ammirati, M. J.; Chrunyk, B. a; Clark, R. W.; Cong, Y.; Culp, J. S.; Danley, D. E.; Freeman, T. B.; Geoghegan, K. F.; et al. Crystal Structure of Cholesteryl Ester Transfer Protein Reveals a Long Tunnel and Four Bound Lipid Molecules. *Nat. Struct. Mol. Biol.* **2007**, *14*, 106–113.

(21) Hamilton, J. A. Fatty Acid Interactions with Proteins: What X-Ray Crystal and NMR Solution Structures Tell Us. *Prog. Lipid Res.* **2004**, *43*, 177–199.

(22) Bruce, C.; Beamer, L. J.; Tall, A. R. The Implications of the Structure of the Bactericidal/permeability-Increasing Protein on the Lipid-Transfer Function of the Cholesteryl Ester Transfer Protein. *Curr. Opin. Struct. Biol.* **1998**, *8*, 426–434.

(23) Kawano, K.; Qin, S. C.; Lin, M.; Tall, A. R.; Jiang, X. C. Cholesteryl Ester Transfer Protein and Phospholipid Transfer Protein Have Nonoverlapping Functions in Vivo . *J. Biol. Chem.* **2000**, *275*, 29477–29481.

(24) Wang, S.; Deng, L.; Milne, R. W.; Tall, A. R. Identification of a Sequence within the C-Terminal 26 Amino Acids of Cholesteryl Ester Transfer Protein Responsible for Binding a Neutralizing Monoclonal Antibody and Necessary for Neutral Lipid Transfer Activity. *J. Biol. Chem.* **1992**, *267*, 17487–17490.

(25) Äijänen, T.; Koivuniemi, A.; Javanainen, M.; Rissanen, S.; Rog, T.; Vattulainen, I. How Anacetrapib Inhibits the Activity of the Cholesteryl Ester Transfer Protein?

Perspective through Atomistic Simulations. *PLoS Comput. Biol.* **2014**, *10*, e1003987.

(26) Mantlo, N. B.; Escribano, A. Update on the Discovery and Development of Cholesteryl Ester Transfer Protein Inhibitors for Reducing Residual Cardiovascular Risk. *J. Med. Chem.* **2014**, *57*, 1–17.

(27) Sikorski, J. A. Oral Cholesteryl Ester Transfer Protein (CETP) Inhibitors: A Potential New Approach for Treating Coronary Artery Disease. *J. Med. Chem.* **2006**, *49*, 1–22.

(28) Liu, S.; Mistry, A.; Reynolds, J. M.; Lloyd, D. B.; Griffor, M. C.; Perry, D. a; Ruggeri, R. B.; Clark, R. W.; Qiu, X. Crystal Structures of Cholesteryl Ester Transfer Protein in Complex with Inhibitors. *J. Biol. Chem.* **2012**, *287*, 37321–37329.

(29) Morris, G. M.; Huey, R.; Lindstrom, W.; Sanner, M. F.; Belew, R. K.; Goodsell, D. S.; Olson, A. J. AutoDock4 and AutoDockTools4: Automated Docking with Selective Receptor Flexibility. *J. Comput. Chem.* **2009**, *30*, 2785–2791.

(30) Frisch, M. J.; Trucks, G. W.; Schlegel, H. B.; Scuseria, G. E.; Robb, M. A.; Cheeseman, J. R.; Scalmani, G.; Barone, V.; Mennucci, B.; Petersson, G. A.; et al. Gaussian 09, Gaussian, Inc, Wallingford CT, **2009**.

(31) Webb, B.; Sali, A. Comparative Protein Structure Modeling Using Modeller. *Curr. Protoc. Bioinformatics.* **2014**, *47*, 5.6.1–5.6.32.

(32) Schuler, L. D.; Daura, X.; van Gunsteren, W. F. An Improved GROMOS96 Force Field for Aliphatic Hydrocarbons in the Condensed Phase. *J. Comput. Chem.* **2001**, *22*, 1205–1218.

(33) Berger, O.; Edholm, O.; Jähnig, F. Molecular Dynamics Simulations of a Fluid Bilayer of Dipalmitoylphosphatidylcholine at Full Hydration, Constant Pressure, and Constant Temperature. *Biophys. J.* **1997**, *72*, 2002–2013.

(34) Koivuniemi, A.; Heikelä, M.; Kovanen, P. T.; Vattulainen, I.; Hyvönen, M. T. Atomistic Simulations of Phosphatidylcholines and Cholesteryl Esters in High-Density Lipoprotein-Sized Lipid Droplet and Trilayer: Clues to Cholesteryl Ester Transport and Storage. *Biophys. J.* **2009**, *96*, 4099–4108.

(35) Siu, S. W. I.; Vácha, R.; Jungwirth, P.; Böckmann, R. A. Biomolecular Simulations of Membranes: Physical Properties from Different Force Fields. *J. Chem. Phys.* **2008**, *128*, 1–12.

(36) Malde, A. K.; Zuo, L.; Breeze, M.; Stroet, M.; Poger, D.; Nair, P. C.; Oostenbrink, C.; Mark, A. E. An Automated Force Field Topology Builder (ATB) and Repository: Version 1.0. *J. Chem. Theory Comput.* **2011**, *7*, 4026–4037.

(37) Vriend, G. WHAT IF: A Molecular Modeling and Drug Design Program. *J. Mol. Graph.* **1990**, *8*, 52–56.

(38) Essmann, U.; Perera, L.; Berkowitz, M. L.; Darden, T.; Lee, H.; Pedersen, L. G. A Smooth Particle Mesh Ewald Method. *J. Chem. Phys.* **1995**, *103*, 8577–8593.

(39) Hess, B.; Kutzner, C.; van der Spoel, D.; Lindahl, E. GROMACS 4: Algorithms for Highly Efficient, Load-Balanced, and Scalable Molecular Simulation. *J. Chem. Theory Comput.* **2008**, *4*, 435–447.

(40) Berendsen, H. J.; Hayward, S. Collective Protein Dynamics in Relation to Function. *Curr. Opin. Struct. Biol.* **2000**, *10*, 165–169.

(41) Natarajan, K.; Senapati, S. Probing the Conformational Flexibility of Monomeric FtsZ in GTP-Bound, GDP-Bound, and Nucleotide-Free States. *Biochemistry.* **2013**, *52*, 3543–3551.

(42) Humphrey, W.; Dalke, A.; Schulten, K. VMD: Visual Molecular Dynamics. *J. Mol. Graph.* **1996**, *14*, 33–38.

(43) Chovancova, E.; Pavelka, A.; Benes, P.; Strnad, O.; Brezovsky, J.; Kozlikova, B.; Gora, A.; Sustr, V.; Klvana, M.; Medek, P.; et al. CAVER 3.0: A Tool for the Analysis of Transport Pathways in Dynamic Protein Structures. *PLoS Comput. Biol.* **2012**, *8*, e1002708.

(44) Laskowski, R. A.; Swindells, M. B. LigPlot+: Multiple Ligand–Protein Interaction Diagrams for Drug Discovery. *J. Chem. Inf. Model.* **2011**, *51*, 2778–2786.

(45) Yung-Chi, C.; Prusoff, W. H. Relationship between the Inhibition Constant (K_I) and

the Concentration of Inhibitor Which Causes 50 per Cent Inhibition (I_{50}) of an Enzymatic Reaction. *Biochem. Pharmacol.* **1973**, *22*, 3099–3108.

(46) Clark, R. W.; Ruggeri, R. B.; Cunningham, D.; Bamberger, M. J. Description of the Torcetrapib Series of Cholesteryl Ester Transfer Protein Inhibitors, Including Mechanism of Action. *J. Lipid Res.* **2006**, *47*, 537–552.

(47) Äijänen, T. Investigation of Interactions between Cholesteryl Ester Transfer Protein and Anacetrapib by using Molecular Simulations. Master of Science Thesis, Tampere University of Technology, Tampere, Finland., **2012**, page 51.

(48) Zhang, L.; Yan, F.; Zhang, S.; Lei, D.; Charles, M. A.; Cavigiolio, G.; Oda, M.; Krauss, R. M.; Weisgraber, K. H.; Rye, K.-A.; et al. Structural Basis of Transfer between Lipoproteins by Cholesteryl Ester Transfer Protein. *Nat. Chem. Biol.* **2012**, *8*, 342–349.

Table 1: Comparison of experimental and theoretical binding energies of the CETP inhibitors. ΔG (experimental) were obtained from the available IC_{50} values using the relation $\Delta G = -RT\, ln(IC_{50})$, under the assumption of noncompetitive inhibition by the studied inhibitors of CETP (see text for details). ΔG (theoretical) values were computed using Autodock program.

Inhibitor	IC_{50} (nm) (Experimental)	$\Delta G_{binding}$ (kcal/mol) (Experimental)	$\Delta G_{binding}$ (kcal/mol) (Theoretical)
Torcetrapib	4.3 (Ref. 21)	-11.4	-10.70
Anacetrapib	7.9*	-11.06	-11.73
BMS-795311	4.0 (Ref. 19)	-11.47	-11.05

*www.selleckchem.com/products/anacetrapib-mk-0859.html

FIGURE LEGENDS

Figure 1. Structures of CETP and its inhibitors: (a) crystal structure of substrate bound CETP (PDB ID: 2OBD) and molecular structures of (b) torcetrapib, (c) anacetrapib, and (d) BMS-795311. The N- and C-terminal domains of CETP are colored in yellow and cyan, respectively. The central domain is shown in red. Functionally relevant loops of CETP: Ω1-Ω6 and bound cholesteryl esters and phospholipids are highlighted. The secondary structural elements are named according to Ref. 20. The central moiety in all the inhibitors is depicted.

Figure 2. Comparison of the residue-level fluctuations of the protein residues in inhibitor and substrate bound states. The figure depicts the root mean square fluctuations of protein residues in substrate (black), torcetrapib (green),anacetrapib (magenta), and BMS-795311 (blue) bound CETP systems. Regions with the most significant changes are labeled, which include the N- and C-terminal distal loops *viz* Ω4- Ω6, Ω1- Ω3, residues of Helix-X and the linker.

Figure 3. Three dimensional representations of the interactions of CETP hydrophobic tunnel residues with (a) torcetrapib, (b) anacetrapib, and (c) BMS-795311. The CETP residues are shown in cyan with the oxygen atoms in red and nitrogens in blue. The hydrogen bonding interaction between anacetrapib and Q199 is shown in black dotted lines with the distance value mentioned. The stacking interaction of F263 phenyl group with one of the middle phenyl rings of the inhibitors is highlighted. The identical interacting residues among the three systems are labelled in red.

Figure 4. Evolution of CETP core tunnel in substrate- and inhibitor-bound states. (a) CETP tunnel radius as a function of tunnel length in substrate bound CETP (black), torcetrapib bound CETP (green), anacetrapib bound CETP (magenta), and BMS-795311 bound CETP (blue). The tunnel reported in substrate bound CETP crystal structure is shown in black dotted line for comparison. Error bars in tunnel radius is included. The 3D representations of the tunnel is shown for (b) substrate-bound CETP and (c) BMS-795311 bound CETP.

Figure 5. Two dimensional representations of the CETP-inhibitor interactions from replica simulations of CETP bound to (a) torcetrapib, (b) anacetrapib, and (c) BMS-795311. Inhibitors are shown in stick representations and the interacting CETP residues are displayed around them. CETP residues that interact *via* hydrophobic/van der Waals interactions are shown by red spikes. The identical interactions among the three systems are depicted by blue circles. Majority of the CETP interacting residues are similar to Fig. 3.

Figure 6. Porcupine plots representing the dominant motions of CETP residues along the first principal component. Results are shown for (a) substrate-bound CETP, (b) torcetrapib bound CETP, (c) anacetrapib bound CETP, and (d) BMS-795311 bound CETP.

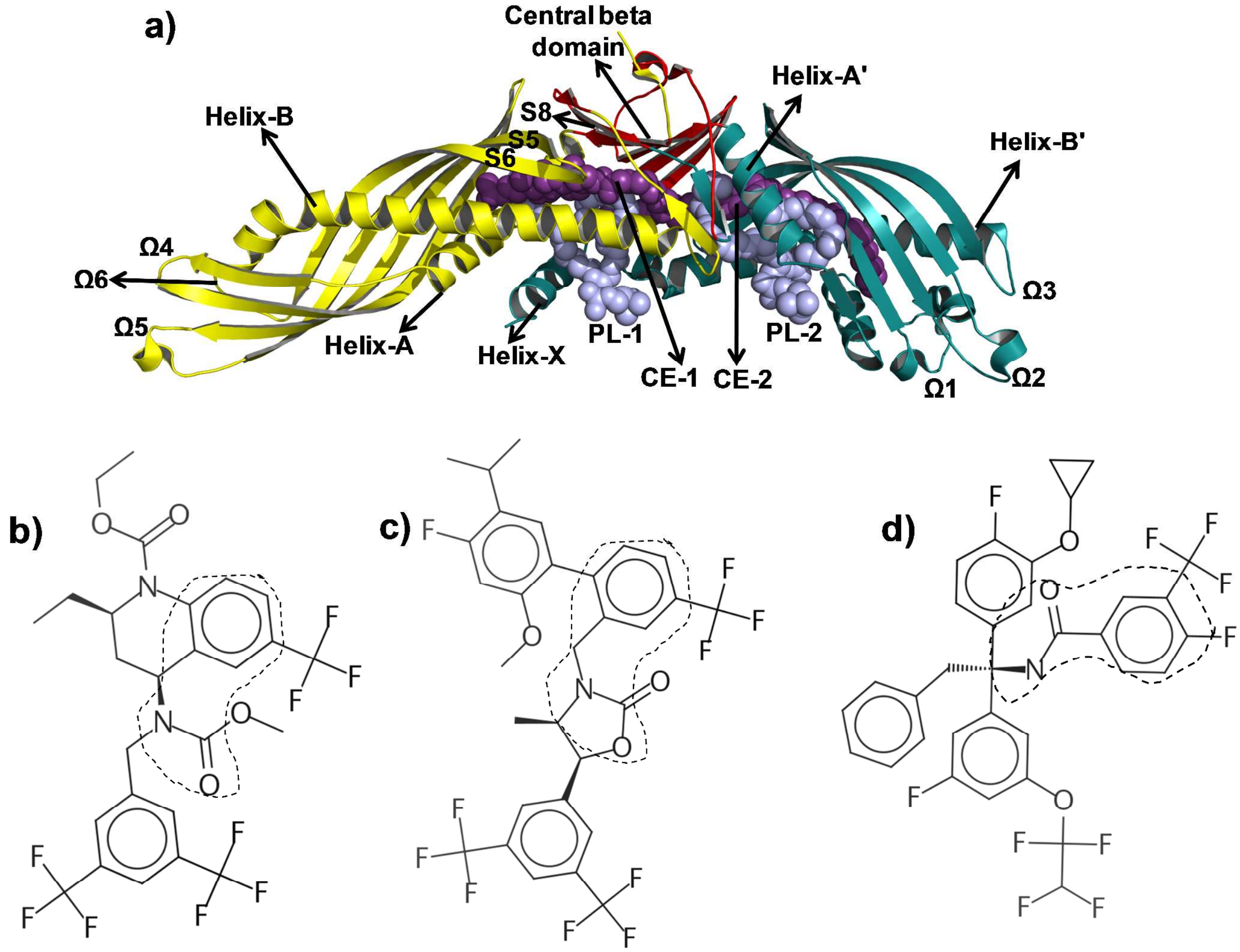
a)
Central beta domain
Helix-A'
Helix-B
S8
S5
S6
Helix-B'
Ω4
Ω6
Ω3
Ω5
Helix-A
Helix-X
PL-1
PL-2
CE-1
CE-2
Ω1
Ω2
b)
c)
d)

Figure 1

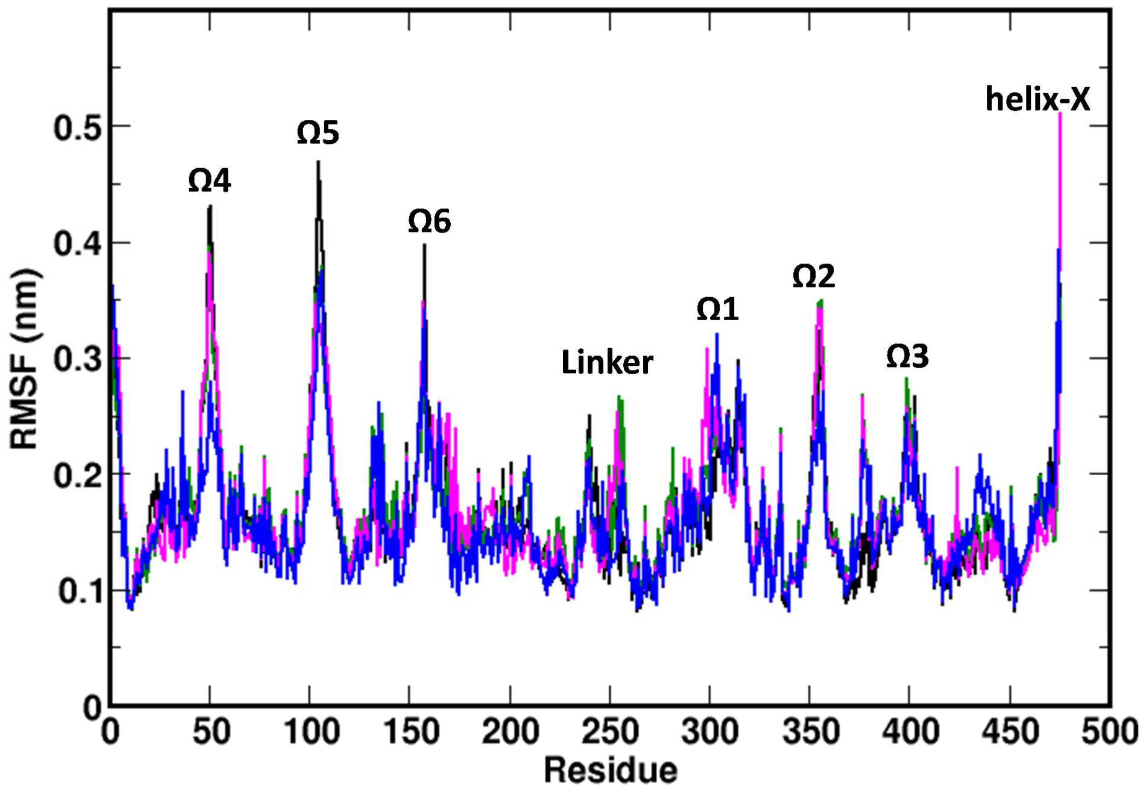
helix-X
Ω5
Ω4
Ω6
Ω2
Ω1
Linker
Ω3
RMSF (nm)
Residue
0
0.1
0.2
0.3
0.4
0.5
0
50
100
150
200
250
300
350
400
450
500

Figure 2

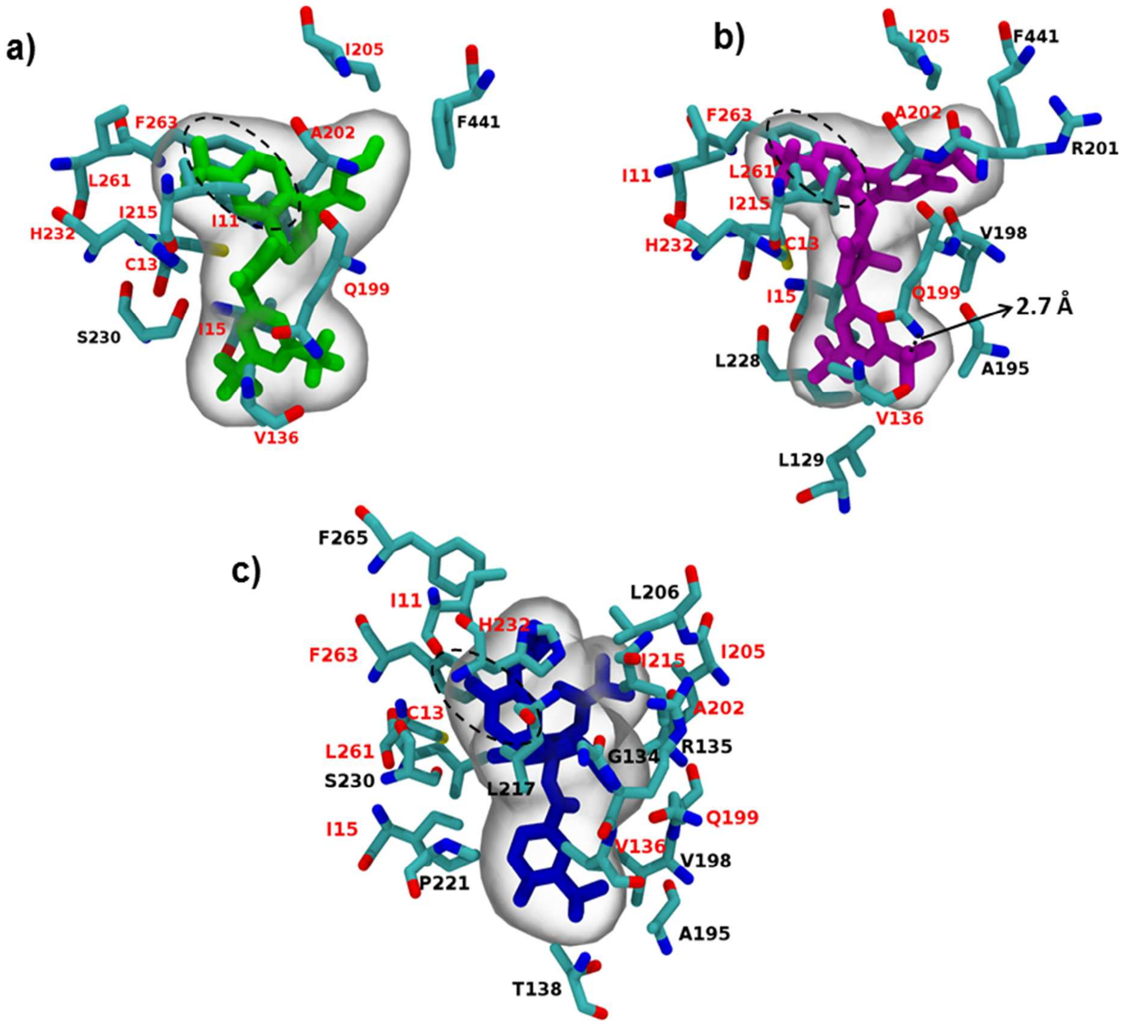
a)
I205
F441
F263
A202
L261
I215
I11
H232
C13
Q199
S230
I15
V136
b)
I205
F441
F263
A202
R201
I11
L261
I215
V198
H232
C13
Q199
I15
2.7 Å
L228
A195
V136
L129
c)
F265
I11
L206
H232
F263
I215
I205
A202
C13
R135
L261
G134
S230
L217
Q199
I15
V136
V198
P221
A195
T138

Figure 3

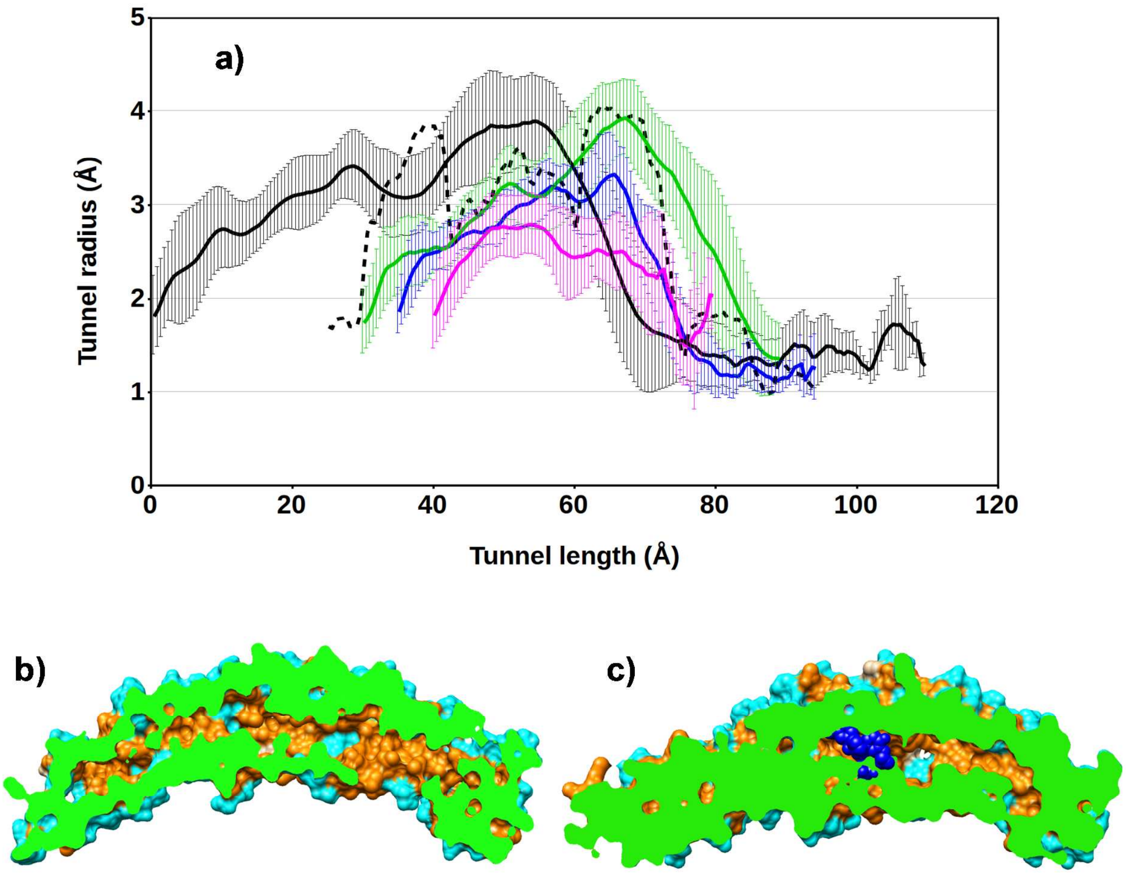
a)
Tunnel radius (Å)
Tunnel length (Å)
0
1
2
3
4
5
0
20
40
60
80
100
120
b)
c)

Figure 4

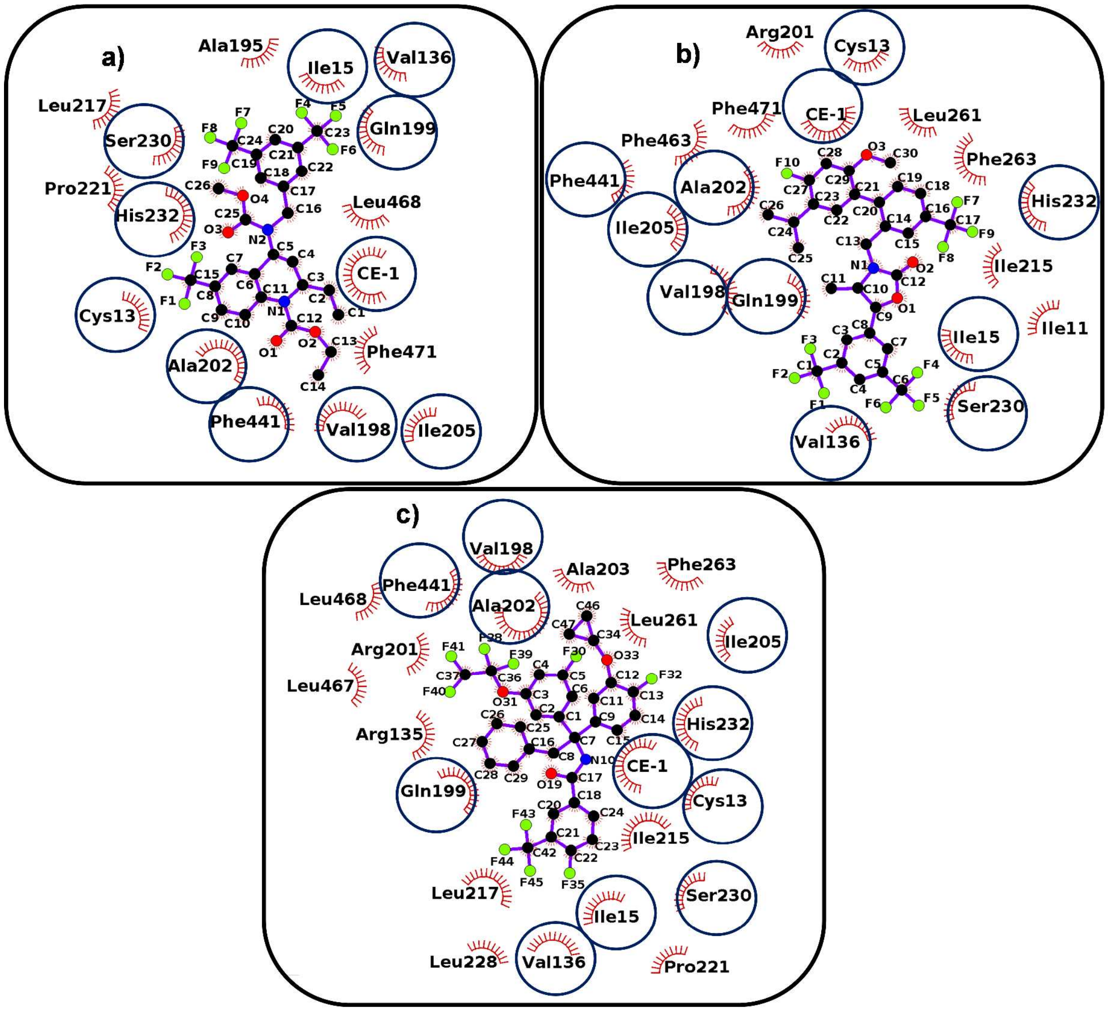

a)
Ala195
Ile15
Val136
Leu217
Ser230
Gln199
Pro221
His232
Leu468
CE-1
Cys13
Phe471
Ala202
Phe441
Val198
Ile205
b)
Arg201
Cys13
Phe471
CE-1
Leu261
Phe463
Phe263
Phe441
Ala202
His232
Ile205
Ile215
Val198
Gln199
Ile15
Ile11
Ser230
Val136
c)
Val198
Phe441
Ala203
Phe263
Leu468
Ala202
Leu261
Ile205
Arg201
Leu467
His232
Arg135
CE-1
Gln199
Cys13
Ile215
Leu217
Ser230
Ile15
Leu228
Val136
Pro221

Figure 5

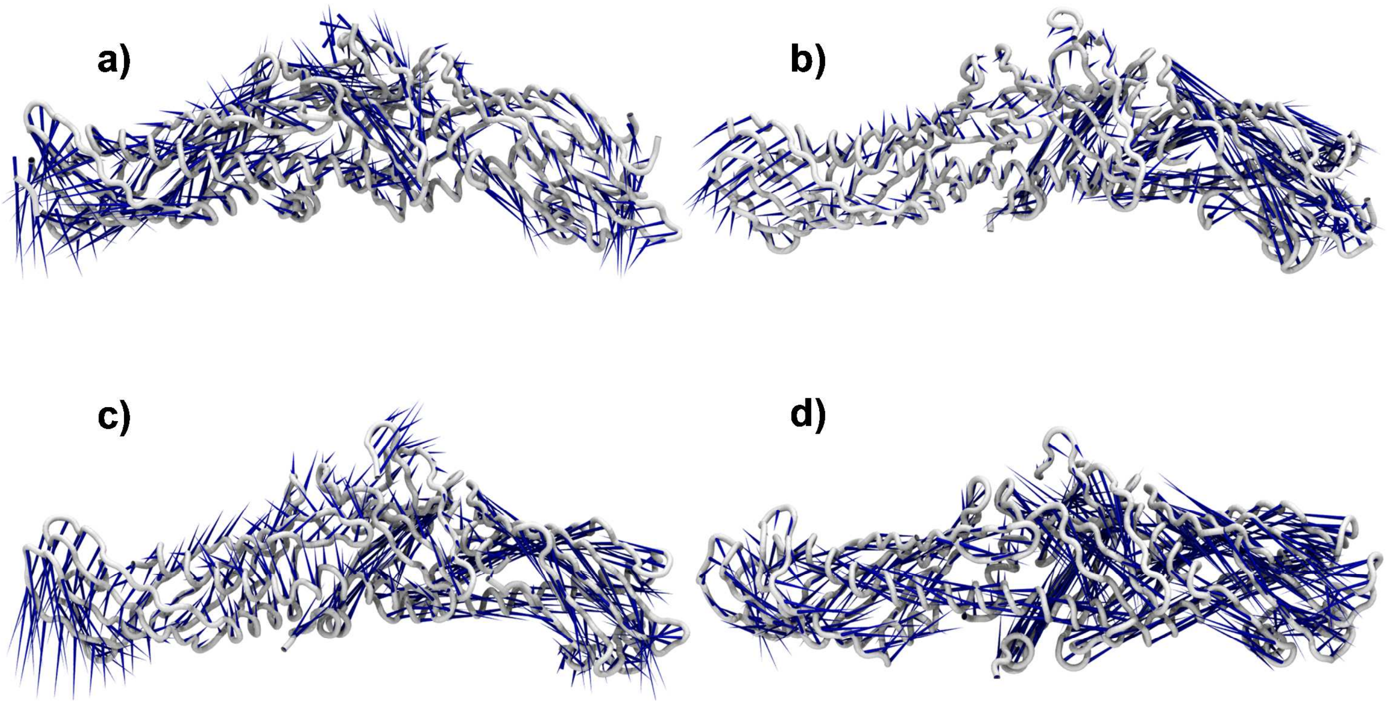

Figure 6

Table of Contents (TOC) Image: